Hybrid LS-DYNA and Python-Based Post-Processing for Long-Range SPH Dispersion Prediction in a Micro MSR Explosion Scenario

Hyoung Tae Kim *, Sung Il Kim
Intelligent Accident Mitigation Research Division, KAERI, Daeduk-daero 989-111, Daejeon, Korea
**Corresponding author: kht@kaeri.re.kr*
Keywords : Molten Salt Reactor (MSR), LS-DYNA, SPH, blast load, drag model, wind effect, hybrid simulation

1. Introduction

Numerical simulations have been widely used to investigate explosion-induced droplet or particle dispersion. However, quantitative prediction of long-range molten salt dispersion inside a truck-mounted micro molten salt reactor (MSR)[1] under internal explosion conditions remains limited.

Explicit fluid–structure interaction simulations covering the entire flight duration are computationally expensive. In particular, LS-DYNA[2] ALE (Arbitrary Lagrangian–Eulerian) – SPH (Smoothed Particle Hydrodynamics)[3,4] coupled simulations are well suited to capture early-time high-pressure acceleration phenomena, but become inefficient when used to compute long-range ballistic motion over several seconds.

To address this limitation, a hybrid computational strategy is proposed. The blast-dominated phase is simulated using LS-DYNA ALE–SPH coupling, while the inertia-dominated ballistic phase is evaluated using a Python-based post-processing model incorporating gravity, quadratic aerodynamic drag, and wind effects.

The objectives of this study are to:

1) Analyze initial molten salt acceleration using ALE–SPH coupling,
2) Develop a post-processing-based long-range dispersion model,
3) Quantitatively evaluate the influence of wind speed and ejection angle on dispersion distance and mass distribution.

2. Hybrid Simulation Methodology

2.1 Micro MSR Explosion Scenario

A missile penetration scenario was assumed for the truck-mounted micro MSR (Fig. 1). The representative condition considered a penetration angle of 45°, consistent with previous studies [5]. The TNT explosive was initialized as a spherical charge corresponding to its mass, with a maximum TNT mass of 200 kg.

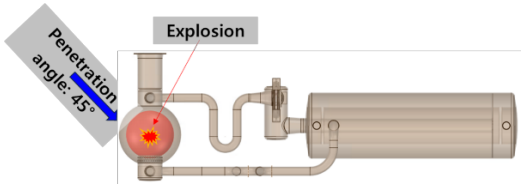

Fig. 1. TNT explosion scenario at the micro MSR.

2.2 Phase Separation Strategy

Molten salt dispersion after TNT detonation is divided into two phases:

1) Blast-dominated phase: high-pressure acceleration immediately after detonation
2) Inertia-dominated phase: ballistic free-flight motion after pressure decay

The blast-dominated phase is computed using LS-DYNA ALE–SPH coupling. Particle data (position, velocity, and mass) are extracted at a transition time t^*=0.2 s, determined based on pressure attenuation and stabilization of particle acceleration.

The inertia-dominated phase is subsequently evaluated using a Python-based ballistic trajectory model [6].

2.3 Definition of SPH Scattered Particles

SPH particle position (x, y, z), velocity (V_x, V_y, V_z), and mass (m) are extracted from LS-DYNA results.

A particle is defined as a scattered particle if:

- It passes through the penetration exit plane, or
- It possesses sufficient outward velocity to escape structural confinement.

The scattering distance is defined as the horizontal distance from the penetration exit center to the first ground intersection.

2.4 Ballistic Post-Processing Model

Particle motion after t^* is governed by:

$$\frac{m_i\, dV_i}{dt} = m_i\, g + F_d\, (V_i + V_w) \qquad (1)$$

where V_i is the particle velocity, g is the gravity, and V_w is the wind velocity.

Quadratic drag (F_d) is applied assuming equivalent spherical particles:

$$F_d = -0.5\, \rho_a\, C_d\, A_i |V_i - V_w|\, (V_i - V_w) \qquad (2)$$

where ρ_a is the air density, C_d is the drag coefficient, and A_i is the effective cross-sectional area of the particle. In this study, A_i was calculated from the diameter equivalent to mass by assuming a particle as an equivalent spherical shape. Time integration is

performed using explicit time stepping (or fourth-order Runge–Kutta).

Table 1 summarizes the reference parameters used for verification.

Table 1: Reference parameters for ballistic model validation

Parameter	Value
C_d (drag coefficient)	0.47
ρ_a (air density)	1.3 kg/m^3
A_i (effective particle area)	0.000490874 m^2
g (gravity constant)	9.81 m/s^2
dt (time step)	0.01 sec
t_{max} (simulation time)	10.0 sec
v_0 (initial velocity)	10.0 m/s
angle (trajectory angle)	45°
$wind_{speed}$ (wind speed)	10 m/s

2.5 Verification of Post-Processing Model

Figure 2 presents verification results of the ballistic model under reference conditions. Under the parameters given in Table 1, wind drag increases the drop distance by approximately 1 m, confirming correct implementation of the drag formulation.

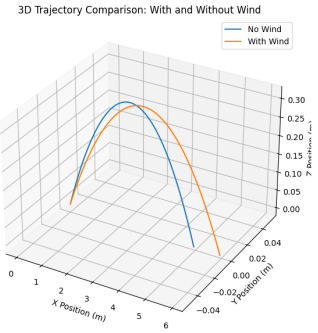

Fig. 2. Verification of ballistic model with and without wind drag.

3. Results and Discussion

3.1 Effect of Wind on Particle Trajectory

Figure 3 shows the effect of wind speed on particle trajectories for different ejection angles.

Without wind, the classical ballistic condition of 45° produces the maximum range. However, as wind speed increases, the effective range becomes increasingly governed by aerodynamic drag and exposure time rather than initial ejection angle. At wind speeds approaching 14 m/s, the difference between 45° and 90° trajectories diminishes significantly.

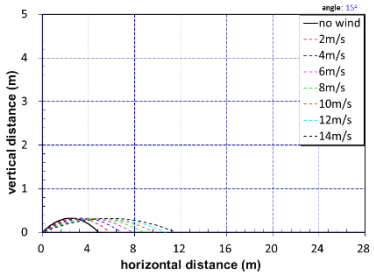

(a) angle: 15°

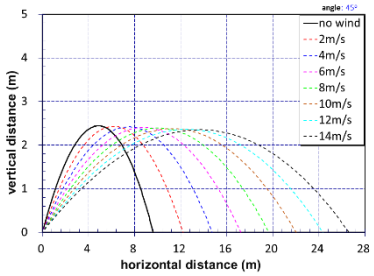

(b) angle: 45°

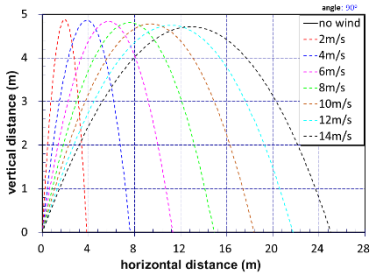

(c) angle: 90°

Fig. 3. Effect of wind speed on SPH trajectory.

3.2 Blast-Dominated Acceleration Behavior

Figure 4 demonstrates molten salt acceleration immediately after TNT detonation.

The blast wave concentrates along the penetration channel, forming a high-velocity jet that transfers momentum to the molten salt. The majority of kinetic energy imparted to SPH particles occurs within the first tens of milliseconds.

This observation confirms that:

- The dispersion potential is primarily determined during the blast-dominated phase.
- Later motion does not significantly alter total mechanical energy, but redistributes particles spatially.

Accurate modeling of early-time pressure and jet formation is critical for realistic dispersion prediction. Over-simplified blast models may lead to substantial underestimation or overestimation of long-range scattering.

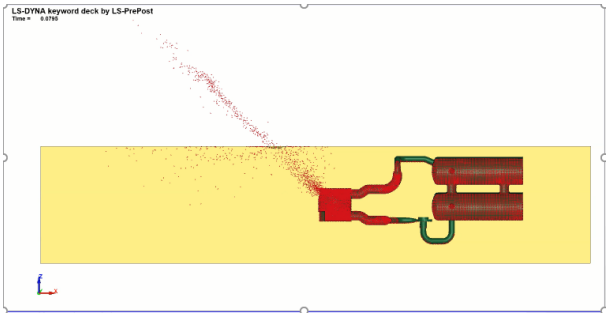

Fig. 4. Molten salt scattering during blast-dominated phase.

3.3 Wind Effect on Scattering Distribution

Figure 5 compares scattering distributions under wind (5 m/s forward) and no-wind conditions.

The maximum scattering distance increased from 899.2 m (no wind) to 981.6 m under wind. However, from an engineering safety perspective, the maximum distance alone is insufficient.

A more meaningful metric is the mass-based cumulative distribution radius, defined as:

- R_{90}: radius containing 90% of dispersed mass
- R_{50}: median dispersion radius

Under wind conditions:

- 90% of molten salt mass is contained within ~123 m
- Without wind, 90% is within ~112 m

Thus, while wind increases maximum range by ~9%, the high-mass containment radius increases by ~10%.

Damage radius assessment should be based on mass-weighted metrics rather than extreme particle distance. The hybrid model enables extraction of such cumulative mass-radius relationships for practical safety evaluation.

The trends of the present scattering distribution are qualitatively consistent with previous studies considering wind-induced dispersion effects [7].

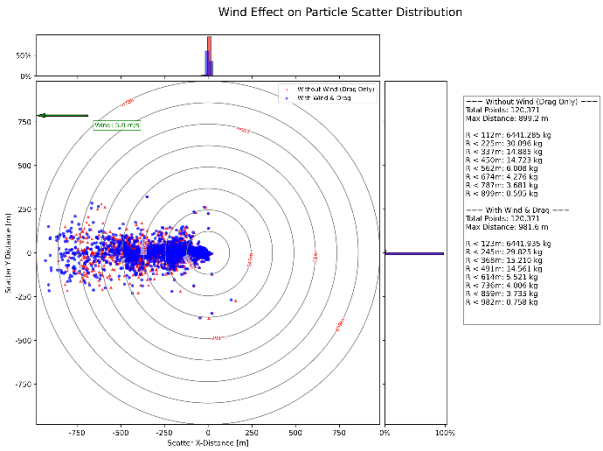

Fig. 5. Comparison of SPH scattering distribution with and without wind (5 m/s forward direction).

4. Conclusions

A hybrid LS-DYNA and Python-based post-processing framework was developed to predict long-range molten salt dispersion under a micro MSR explosion scenario.

Key engineering findings are:

1) Blast-dominated acceleration controls dispersion potential.

Most kinetic energy transfer occurs within tens of milliseconds, emphasizing the importance of accurate ALE–SPH coupling.

2) Wind significantly modifies dispersion behavior.

For the 200 kg TNT, 45° penetration case, maximum scattering distance increased from 899 m to 982 m under a 5 m/s wind condition.

3) Mass-based dispersion metrics provide more meaningful safety indicators than maximum range alone.

The 90% mass containment radius increased from 112 m to 123 m under wind conditions.

4) The phase-separated hybrid approach achieves computational efficiency while maintaining physical consistency.

Long-duration explicit simulation is avoided without compromising trajectory realism.

From a safety engineering perspective, the proposed framework enables:

- Quantitative estimation of dispersion radius under varying wind conditions
- Rapid sensitivity analysis for accident scenario evaluation
- Practical support for damage radius and emergency planning assessment

Future work will extend the model to include structural deformation (FSI) and multiphase radioactive transport.

ACKNOWLEDGMENTS

This work was supported by Korea Research Institute for defense Technology planning and advancement(KRIT) grant funded by the Korea government(DAPA(Defense Acquisition Program Administration)) (KRIT-CT-22-017, Next Generation Multi-Purpose High Power Generation Technology(Liquid Fuel Heat Generator Transportation and Safety Assessment Technology), 2022).

REFERENCES

[1] “Status of Molten Salt Reactor Technology”, Technical Reports Series No. 489 (STI-DOC-010-489), International Atomic Energy Agency Vienna, Nov. 2023.
[2] ANSYS Inc., LS-DYNA Keyword User’s Manual R15, Feb. 2024.

[3] L. B. Lucy, A numerical approach to the testing of the fission hypothesis, The Astronomical Journal 82, pp.1013-1024, 1977.

[4] R. A. Gingold and J.J. Monaghan, Smoothed particle hydrodynamics: theory and application to non-spherical stars, Monthly Notices of the Royal Astronomical Society, 1977.

[5] H.T. Kim and S.I. Kim, LS-DYNA Calculation of Blast Load on the Micro Molten Salt Reactor Designed to Fit on a Truck, Transactions of the Korean Nuclear Society Autumn Meeting Changwon, Korea, October 24-25, 2024.

[6] H.T. Kim and S.I. Kim, Development of a Post-Processing Program based on LS-DYNA Code for SPH Particle Dispersion Analysis, Technical Report of Korea Atomic Energy Research Institute, KAERI/TR-11389/2025.

[7] J.H. Shin, G.H. Gim, S.M. Chang, Y. Seo, B. Lee, and S. Nam, On the Effect of Wind in the Extinguishing System for Wild Forest Fire, Journal of the Korean Society of Hazard Mitigation, Vol. 14, No. 2, pp. 169-176. 2014.